Chapter 4
Chiral nematics confined in spheroids

The results presented in this chapter are to be submitted as a paper to **Soft Matter** under the title *"Hybridization and stability of blue phases via geometrical frustration"*.

Blue phases consist in a highly chiral liquid crystal that forms networks of defect lines spontaneously, often with some cubic symmetry [169]. The applicability of liquid crystals ranges from low energy displays [15] to optical detection devices [27, 34, 35] and most recently the development of photonic crystals [170, 10, 171, 85]. Blue phases are attractive because of their fast response to external stimuli [172, 173]. However, their stability is subject to small changes of temperature which has proven to be a challenge for technological applications. Efforts towards their stabilization focus mainly on doping nematic phases [51–58] but its optimization remains to be an open problem.

It is possible to generate a new family of defect configurations by geometrical frustration, this is creating a competition between the surface and elastic free energy [174]. When confined in channels, cholesteric liquid crystals form structures similar to skyrmions and patterns on the surface [175–177]; in droplets it is possible to reproduce the order of BPs or take advantage of the intricate topology of chiral nematics and form knots to braid nanoparticles [178, 179, 87, 180–182, 86, 183].

A phase diagram for micron size droplets of chiral LCs has been reported [182] showing an ample variety of configurations like twist cylinder (TC), radial spherical structure (RSS), blue phase I

(BPI) and blue phase II (BPII). Some regions of the phase diagram are in agreement with reports from bulk systems [184, 185]. The stability of each region was determined by comparing the total free energy of different Ginzburg–Landau relaxations of ansatz configurations.

From molecular simulations it is known that a freely suspended droplet morphs to prolate shape domains, a deformation caused by the shape of the molecules[186]. The formation of non-spherical droplets is also known for lyotropic liquid crystals [187–190]. The anisotropy of these geometries induces chirality with a certain range of stability. Mechanical deformation of BPI has been reported in order to tune optical response through an applied strain [17, 191], providing a different avenue for the fabrication of low-voltage electro-optic devices. By observing results of the phases in different geometries and the effect of strain in BP, we endeavor to ellucidate the effect of curvature in confined LCs with different chiralities. Is it possible to stabilize phases by means of physical constrains instead of chemical alteration of the material?

To achieve this, three different types of spheroids were set: oblates, spheres, and prolates. A droplet of 500 nm radius was set as the base geometry, and the dimensions were modified to obtain isochoric domains with different aspect ratios $\varphi = {}^{c}/_{a}$, being c and a the lengths of the semi-principal axes aligned with the z and x Cartesian axes respectively. For $\varphi < 1$ the geometries are called oblates, and for $\varphi > 1$ they are called prolates. The case of a sphere is reproduced by setting $\varphi = 1$. Additionally, for all geometries the cross section parallel to the xy plane is a perfect circle with radius R. The three types of geometries are illustrated in figure 4.1.

The thermodynamic model that was used for this set of simulation follows the descriptions introduced in chapter 2, and the equilibrium configurations were found by employing a theoretically informed Monte Carlo method presented in section 2.3.2 with a FEM implementation for the geometry discretization in section 2.2.2.

The next section is dedicated to the analysis of the results which is divided into the free energy perspective of the simulations, phase diagrams for the different geometries, and a section for additional details of confined chiral nematics that should be highlighted.

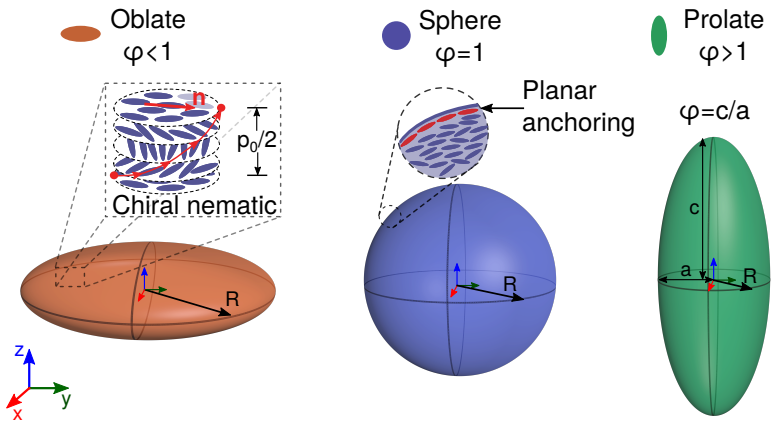

Figure 4.1. Schematic of the types of geometries. (Left) Oblate spheroid, $\varphi < 1$. The insert shows an schematic of the behavior of a chiral nematic, where p_0 is the cholesteric pitch and $\mathbf{n}$ is the mean molecular orientation or director vector. (Center) Sphere, $\varphi = 1$. The insert shows the planar alignment of the molecules at the surface. (Right) Prolate spheroid, $\varphi > 1$. The aspect ratio φ is defined by the lengths c and a which are aligned with the Cartesian directions z and y. The cartoons next to each spheroid will be used throughout this chapter to represent the geometry.

4.1 Results

The chiral liquid crystal was modelled with parameters of nematic coherence length $\xi_N = \sqrt{L_1/A} = 10$ nm, and splay elastic constant $k_{11} = 16$ pN. The systems were confined with strong ($W = 1 \times 10^{-3} J/m^2$), moderate ($W = 1 \times 10^{-4} J/m^2$), and weak ($W = 1 \times 10^{-5} J/m^2$) anchoring strength. The imposed molecular orientation at the surface is planar degenerate.

The chirality is controlled with the adimensional parameter $N = 4R/p_0$, indicating the number of π-turns the director makes along a distance R. In order to build consistent phase diagrams for all geometries, we calculate the pitch necessary to keep N constant as φ varies. The phase diagrams are built in terms of the inverse reduced temperature $\tau = 9\,(3 - U)\,/U$ and the chirality parameter N that spans from low chirality ($N \leq 2$) to high chirality ($N \geq 3$).

We start this discussion by studying the changes in the three contributions of the free energy for a scenario with strong anchoring conditions and at a fixed temperature, see figures 4.2–4.4. The dominance of chirality and its consequences in the final configuration of the system is evident from the free energies. Then, from the complete set of results we are able to build phase diagrams for the three families of geometries and analyze how curvature effects and anchoring conditions

modify stability regions and characteristics of the equilibrium configurations, see figures 4.5–4.7. At the end, we highlight three phenomena that occur on specific regions of the phase diagram with an special interest on the adaptation of blue phases as φ changes.

4.1.1 Free energy analysis

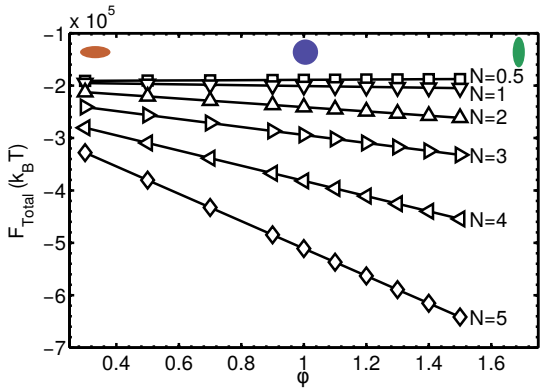

Figure 4.2. Total free energy in function of the aspect ratio, φ, for strong anchoring $W = 1 \times 10^{-3} J/m^2$ and $U = 2.9$. Different markers indicate the chirality through the parameter N. The cartoons in the top of the figure indicate the type of spheroid.

Figure 4.2 shows the total free energy for different chiralities and aspect ratios. As chirality increases, the associated elastic term dominates over the other contributions resulting in a monotonic decrescent tendency. It is important to note that the surface of the tactoids is rigid and there is no possible deformation of the geometry beyond that established by φ. The minimum of the total free energy is not necessarily reached by increasing φ, as apparently happens in figure 4.2. Recall that for the same value of N, prolates have a smaller pitch than an oblate, and for $N > 3$ we expect to observe blue phases. In those cases, a change in the free energy is interpreted as a drastic change in the nature of the defect network as we will show in the phase diagrams. To study the complete effect of curvature and chirality, we separate each contribution of the free energy.

Figure 4.3 shows the Landau–de Gennes free energy and surface free energy. These two contributions follow the same behavior as chirality and φ increase. The monotonic behavior of the bulk free energy as chirality increases (purple arrow in figure 4.3) is a consequence of the formation of defects. Note that for all cases with $N < 2$, where pitch values vary between $850\ nm$

and $6\ \mu m$, this component of the free energy is constant. The systems exhibit a cholesteric configuration identified by the continuous twist of the director field so the distribution of the scalar order parameter in the bulk is uniform. For highly chiral systems, the defect density increases dramatically and so the change in the local nematic order is more abrupt. The effect of φ (blue arrow in figure 4.3) translates to an increase in the dimensions in the z-direction so it fits more nematic layers, thus increasing the Landau–de Gennes energy.

For the surface free energy, see figure 4.3, the only defects for low chirality are two surface boojums and are present in all geometries. For shorter pitch, the networks of disclination lines are distributed throughout the bulk and touch the surface forming a Schlieren-like texture or patterns composed of various $\lambda^{-1/2}$ and λ^{+1} rotations of the director field. The surface area is minimized when $\varphi = 1$, as shown in the insert, but although the oblate has the maximum surface area it also shows the largest patterns.

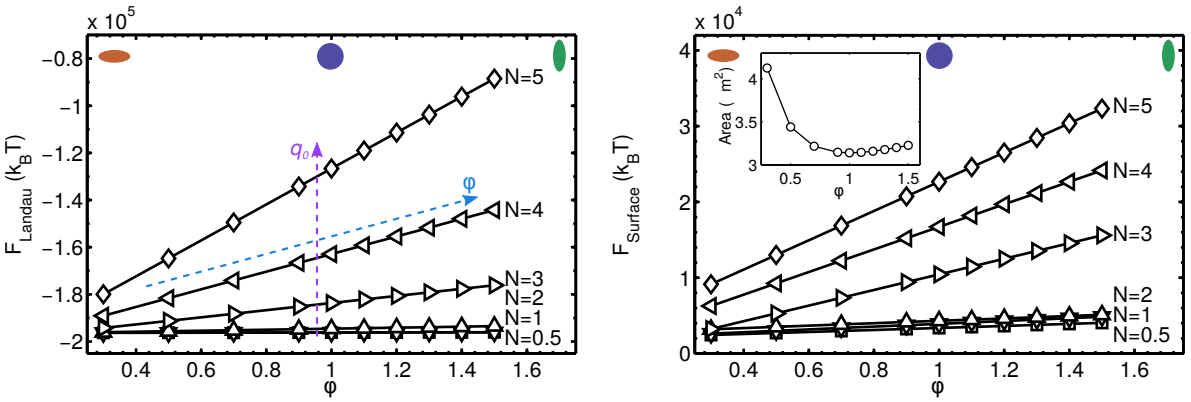

Figure 4.3. (Top) Landau–de Gennes free energy and (Bottom) surface free energy in function of the aspect ratio, φ, for strong anchoring $W = 1 \times 10^{-3} J/m^2$ and $U = 2.9$. The insert shows the surface area for different φ and constant volume.

The total elastic free energy and the gradients of the chiral term are shown in figure 4.4. The decrescent character of this contribution is caused by the dominance of the chiral term led by the elastic constant L_5. The elastic constant L_5 is directly proportional to the inverse pitch q_0, so smaller pitch values mean a greater energetic penalty for twist deformation making the chiral term more dominant in prolates than oblates.

For each curve of N, we observe a plateau in the gradients of the chiral term in the bottom of figure 4.4. By removing the changing value of p_0 we note there is a cutoff aspect ratio for each chirality, indicating that the final configuration will not change beyond a certain value of φ. This is more clear if we observe the curve for $N = 0.5$, which shows a TwBs phase or TC. For prolates, there are two well–defined poles that help preserve the same bispherical characteristic of the phase in a droplet. For high chirality, the plateau is not evidenced which indicates the characteristics of the configuration change between cases.

In summary, for low chirality the equilibrium configuration is similar between geometries and the only indicative of a preferred geometry is induced by a slight twist of the director field. As chirality increases, prolates induce a more intricate network of defects which results in penalization on all the contributions of the free energy.

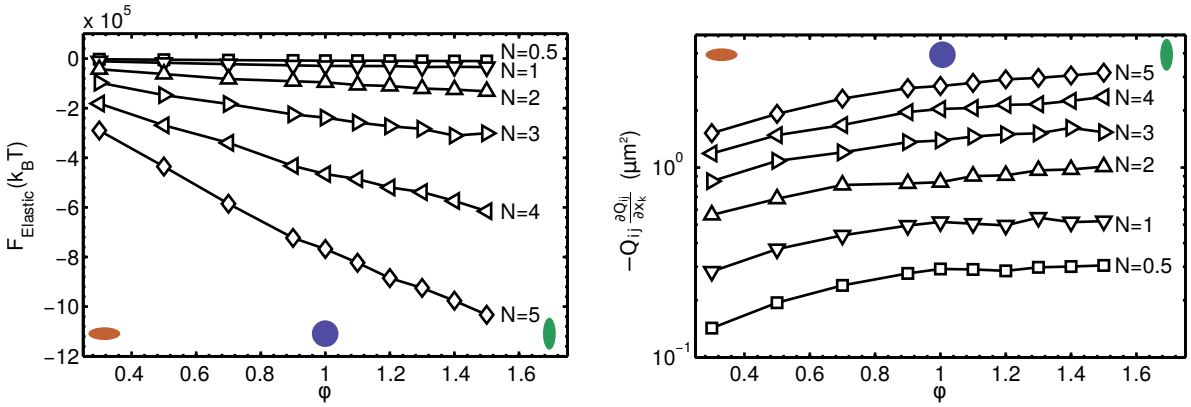

Figure 4.4. Elastic free energy in function of the aspect ratio, φ, for strong anchoring $W = 1 \times 10^{-3} J/m^2$ and $U = 2.9$.

Now that the phenomenology of the free energy has been described, we proceed to present the effects that different interplays have on the equilibrium configurations of the tactoids. First, phase diagrams for the three types of geometries as the anchoring is weakened show how morphologies are transformed or suppressed. In the alternate geometries, some phases persist or rearrenge expanding the family of possible configurations. There are some special cases that we shall examine in more detail at the end of this section.

4.1.2 Phase diagram: Droplet

The phase diagram for a $\varphi = 1$ geometry with strong anchoring conditions is shown in figure 4.5A. In this diagram we can observe two families of phases: one dictated by the surface ordering, and other dictated by the bulk. When the surface dominates, the phases are Bipolar (B), Twisted Bipolar (TwBs), and Radial Spherical Structure (RSS). The blue phases (BPI and BPII) are configurations where the bulk dominates over the surface and defect structures within the droplet are present.

For non-chiral materials, the formation of a bipolar phase is predicted and characterized by the formation of two surface boojums connected by symmetrical director field lines. If chirality increases, the boojums are preserved in opposite poles as the director field twists inside the droplet in a helical fashion; this phase is called Twisted Bipolar (TwBs). For low temperatures ($\tau < 0$), the phase is somehow frozen and the two surface defects are preserved. However, the boojums attract each other to satisfy the twisting of the director field so they are not located in opposite poles. Eventually the two boojums combine in one single surface defect that ties a knot defect in the bulk following a Frank-Prize like structure.

The bulk-dominated phases are present at high temperatures ($\tau > 0$) and high chirality regions. The structures are characterized by the formation of a network of disclination lines. When the systems are not confined, the network follows a cubic symmetry and are reported in the literature as Blue Phase II (BPII) with a O_2 symmetry, and Blue Phase I (BPI) with O_8 symmetry. For confined phases the periodicity of the structure is interrupted, and specifically for curved surfaces the defect lines bend and deform the shape of each cell. We differentiate the blue phases as BPII if the defect lines merge in the center of the cell (blue higlights in (e)) or BPI if such defects avoid each other (green lines in (f)). Although the defects are highly bent, the surface structure forms a regular hexagonal pattern composed of an array of $\lambda^{-1/2}$ and λ^{+1} disclinations. These defects are typical of cholesteric phases where there is no abrupt change in the molecular orientations. The hexagons are better defined for a narrow interval of temperatures that coincide with the stability region of the BPII. As the temperature is lowered, the pattern presents more red regions where molecules satisfy the anchoring conditions.